



OPEN ACCESS

EDITED BY
Umar Khan,
Hazara University, Pakistan

REVIEWED BY
Basharat Ullah,
Mohi-Ud-Din Islamic University,
Pakistan
Zulqurnain Sabir,
United Arab Emirates University, United
Arab Emirates

*CORRESPONDENCE
Arshad Khan,
arshad8084@gmail.com

SPECIALTY SECTION
This article was submitted to Process
and Energy Systems Engineering,
a section of the journal
Frontiers in Energy Research

RECEIVED 13 July 2022
ACCEPTED 02 September 2022
PUBLISHED 06 October 2022

CITATION
Khan A, Alyami MA, Alghamdi W,
Alqarni MM, Yassen MF and Tag Eldin E
(2022), Thermal examination for the
micropolar gold–blood nanofluid flow
through a permeable channel subject to
gyrotactic microorganisms.
Front. Energy Res. 10:993247.
doi: 10.3389/fenrg.2022.993247

COPYRIGHT
© 2022 Khan, Alyami, Alghamdi, Alqarni,
Yassen and Tag Eldin. This is an open-
access article distributed under the
terms of the [Creative Commons
Attribution License \(CC BY\)](https://creativecommons.org/licenses/by/4.0/). The use,
distribution or reproduction in other
forums is permitted, provided the
original author(s) and the copyright
owner(s) are credited and that the
original publication in this journal is
cited, in accordance with accepted
academic practice. No use, distribution
or reproduction is permitted which does
not comply with these terms.

Thermal examination for the micropolar gold–blood nanofluid flow through a permeable channel subject to gyrotactic microorganisms

Arshad Khan^{1*}, Maryam Ahmed Alyami², Wajdi Alghamdi³,
M. M. Alqarni⁴, Mansour F. Yassen^{5,6} and Elsayed Tag Eldin⁷

¹College of Aeronautical Engineering, National University of Sciences and Technology (NUST), Islamabad, Pakistan, ²Department of Mathematics, Faculty of Sciences, University of Jeddah, Jeddah, Saudi Arabia, ³Department of Information Technology, Faculty of Computing and Information Technology, King Abdulaziz University, Jeddah, Saudi Arabia, ⁴Department of Mathematics, College of Science, King Khalid University, Abha, Saudi Arabia, ⁵Department of Mathematics, College of Science and Humanities in Al-Aflaj, Prince Sattam Bin Abdulaziz University, Al-Aflaj, Saudi Arabia, ⁶Department of Mathematics, Faculty of Science, Damietta University, Damietta, Egypt, ⁷Faculty of Engineering and Technology, Future University in Egypt New Cairo, New Cairo, Egypt

Presently, scientists across the world are carrying out theoretical and experimental examinations for describing the importance of nanofluids in the heat transfer phenomena. Such fluids can be obtained by suspending nanoparticles in the base fluid. Experimentally, it has proved that the thermal characteristics of nanofluids are much better and more appealing than those of traditional fluids. The current study investigates the heat transfer for the flow of blood that comprises micropolar gold nanoparticles. The influence of chemically reactive activation energy, thermophoresis, thermal radiations, and Brownian motion exists between the walls of the channel. A microorganism creation also affects the concentration of nanoparticles inside the channel. Suitable transformation has been used to change the mathematical model to its dimensionless form and then solve by using the homotopy analysis method. In this investigation, it has been revealed that the linear velocity behavior is two-folded over the range $0 \leq \eta \leq 1$. The flow is declining in the range $0 \leq \eta \leq 0.5$, whereas it is augmenting upon the range $0.5 \leq \eta \leq 1$. Thermal characteristics are supported by augmentation in volumetric fraction, thermophoresis, radiation, and Brownian motion parameters while opposed by the Prandtl number. The concentration of the fluid increases with augmentation in activation energy parameters and decays with an increase in

Abbreviations: \hat{u} , \hat{v} , dimensional velocity components (m/s); \hat{p} , dimensional pressure (Pa); P , dimension-free pressure; H , channel height (m); N , microrotational velocity (m/sec); u_t , u_b , velocities of the top and bottom walls (m/sec); v_t , v_b , normal velocities of the top and bottom walls (m/sec); T , dimensional temperature (K); C_p , specific heat ($Jkg^{-1}K^{-1}$); Nu , Nusselt number; C_f , skin friction coefficient; Sh , Sherwood number; N_b , Brownian parameter; η , similarity variable; Re , Reynolds number; Da , Darcy number; Pr , Prandtl number; K , material parameter; R_d , radiation parameter; Ω , temperature parameter; E , activation energy parameter; Sc , Schmidt number; I , chemical reaction parameter; L_b , bioconvection Lewis number; Pe , Peclet number; δ , microorganism concentration number; N_t , thermophoresis parameter.

thermophoresis, Brownian motion, chemical reaction parameters, and the Schmidt number. The density of microorganisms weakens by growth in Peclet and bioconvection Lewis numbers.

KEYWORDS

heat transfer, micropolar nanoparticles, gyrotactic microorganisms, porous channel, chemical reaction, thermal radiation, HAM

1 Introduction

The limitations on improving the transfer of heat in engineering systems, for instance, cooling of electronic and solar systems, are essentially due to the slower thermal conductivity in traditional fluids like oil, ethylene glycol, and water. Solids normally have better characteristics for heat transmission than liquids, like copper which has 700 times better thermal conductivity in comparison with water and 3,000 times better than engine oil. Choi and Eastman (1995) were the first to introduce the concept of nanofluids by mixing the nano-sized particles in a pure fluid. Afterward, various researchers have conducted plenty of investigations for fluids flowing through channels with the main focus on the augmentation of heat transfer characteristics by suspending different kinds of nanoparticles in different base fluids. Sheikholeslami and Ganji (2013) have discussed the thermal flow characteristics for the $Cu - H_2O$ nanofluid flow amid two parallel plates. In this study, the Maxwell–Garnets and Brinkman models have been employed by the authors to determine the viscosity and thermal flow behavior of nanofluids. It has also been established in this inspection that the rate of thermal flow has amplified with greater values of the volumetric fraction and Eckert number. Ayub et al. (2022a) have inspected the thermal flow characteristics for cross-nanofluids by using various flow conditions and revealed that augmentation in the cross-fluid index has supported velocity profiles. Shah et al. (2022a) have inspected the MHD nanofluid flow with multiple features past wedge geometry. Shah et al. (2020) have extended the study of Srinivas et al. (2017) by introducing the micropolar gold–blood nanofluid to the flow system in a channel. They have used the homotopy analysis method to model equations and have revealed that the thermal flow has improved for higher values of the volumetric fraction and radiation parameter which, on the other hand, has declined the flow profiles in all directions. Further investigation about heat transmission regarding nanofluids can be studied in Ayub et al. (2021a), Ayub et al. (2021b), Ayub et al. (2021c), Shah et al. (2021), Ayub et al. (2022b), Shah et al. (2022b), and Ayub et al. (2022c).

The fundamental requirement to model the fluid that comprises microrotational components has introduced the theory of micropolar fluids. These fluids actually couple the rotational motion of fluid particles with the field of macroscopic velocity. By structure, these fluids consist of hard particles suspended in the viscous medium, for instance, bubbly

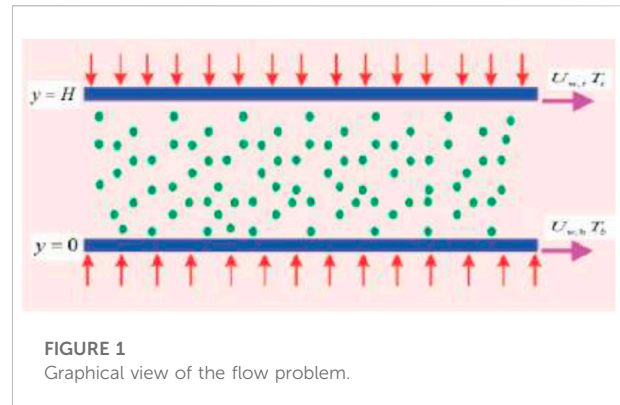
liquid, paint, ferrofluids, and blood flows. Such fluids have abundant applications in engineering and industries, like lubricant fluids, biological structures, and polymer solutions. The idea of micropolar fluids was introduced first by Eringen (1966). Afterward, this term became an area of dynamic exploration in the field of research. This class of fluid could describe the fluid's characteristics at a micro-scale. In these fluids, the spinning motion is described by microrotational vectors. Singkibud et al. (2022) have investigated the influence of cubical catalyst-based activation energy and thermophoresis diffusions for a time-free micropolar nanofluid flow on a semi-infinite stretching surface. Fakour et al. (2015) inspected the thermal flow of micropolar fluids flowing through a channel. It has been concluded in this investigation that the rate of thermal flow has augmented with growth in the strength of the Reynolds number and has declined with augmentation in the Peclet number. Abbas et al. (2020) have revealed thermal characteristics for the micropolar nanofluid flow between two plates using slip conditions. Baharifard et al. (2020) studied the mass and heat transfers for the MHD micropolar fluid flow past a stirring surface with injection and suction behavior on the surface.

Recently, the exploration of the laminar flow and transmission of heat through porous channels has appealed to many researchers due to its industrial and biological applications. These applications include biological fluid transportation through contracting or expanding vessels, underground resources of water, and the synchronous pulsation of permeable diaphragms. Many investigations have been conducted for heat and mass transfer between porous plates using various flow conditions. In this study, magnetic effects have been practiced in the flow system both in parallel and perpendicular directions, and it has been highlighted that by removing the impact of the Hall current, the flow has remained unchanged even by changing the direction of the applied magnetic field. Hassan (2020) has analyzed the production of irreversibility for the MHD fluid flowing in a permeable channel. Islam et al. (2020) have examined the micropolar fluid flow amid two plates by considering different flow conditions in the flow system. The authors have used the nanoparticles of graphene oxide and copper in water as the base fluid and have established that the expansion in volumetric fractions has reduced the flow characteristics and has increased the thermal characteristics. Delhi Babu and Ganesh (2020) have

discussed mathematically the model for the steady MHD fluid flow amid two porous plates with revolving flow.

Nanoparticles are not self-driven and start motion only when it is affected by thermophoresis and Brownian motion. Even in the augmentation of mass and heat transformation, the high concentration of nanoparticles can affect the stability of this phenomenon. A combination of biotechnological mechanisms with nanofluids that are established by motile microorganisms can provide better results in such a physical phenomenon. Gyrotactic microorganisms are actually self-driven and can gather in the closed vicinity of the top layer of the fluid flow which causes the upper surface of the fluid to be denser. The dispersal of gyrotactic microorganisms in nanofluids normally enhances the heat transfer characteristics of the fluid. Platt (1961) was the first gentleman who floated the idea of the configurations in the thicker culture of free spinning organisms. Afterward, many studies have been carried out by different scientists with the main focus on the impact of gyrotactic microorganisms on the fluid flow systems. Bin-Mohsin et al. (2017) have examined the squeezing liquid flow using gyrotactic microorganisms amid two opposite and parallel plates. It has been highlighted in this investigation that the augmentation in thermophoresis effects and random motion has enhanced the thermal flow and has declined the mass transmission. Zhang et al. (2020) studied the influence of the magnetized Reynolds number upon motile microorganisms between circular plates filled with nanoparticles. The authors have noticed that the distribution of nanoparticle concentration, thermal profiles, and microorganisms have been highly suppressed by augmenting values of the squeezed Reynolds number. Ahmad et al. (2020) inspected the nanofluid flow influenced by microorganisms through a porous plate. It has been noticed in this investigation that the heat and mass transfer rates have been augmented by considering the impact of gyrotactic microorganisms. More comprehensive investigations have been conducted by Khan et al. (2021a) and Khan et al. (2021b). The authors have highlighted the effect of different parameters on flow systems. In these inspections, it has been noticed that the flow and concentration profiles have been reduced with augmentation in thermophoretic and Brownian motion parameters, while the thermal profiles have been augmented on the other hand. Moreover, in these investigations, the density number of motile microorganisms has declined with the augmenting values of the Peclet number.

From the mentioned literature and similar related studies, the authors have noticed that a large number of research studies have been published to describe the flow of nanoparticles by using different geometrical shapes. However, comparatively less attention has been paid to micropolar fluids with gold–blood nanoparticles flowing through the channel. Moreover, to the best of the author’s knowledge, no investigation so far has been



performed for micropolar gold–blood nanoparticles flowing through a porous channel with the effects of gyrotactic microorganisms. The collective influence of chemically reactive activation energy in the current study further expands the newness of the study. For augmenting the heat transfer characteristics in the current investigation, the thermophoretic effects along with Brownian motion and thermal radiations have also been applied to the flow system. HAM (Liao, 1999; Liao, 2010) has been used to find the solution to modeled equations.

The first section of the study introduces the related literature. The second section comprises physical and mathematical description of the problem along with quantities of interest. The third section defines the solution method along with steps for the solution. The fourth section defines the results and discussion along with an explanation of tables. Conclusions of the current study are given in the last section.

2 Physical and mathematical descriptions

Next, the problem will be described physically by considering some assumptions and by taking the physical view of the flow problem. Afterward, these assumptions will be employed to describe the problem in the mathematical form. This mathematical description will then be transformed into the dimensionless form with the help of similarity variables. In this process, some physical parameters will be recovered that will be discussed briefly along with mathematical expressions at the end of the section.

2.1 Physical description

A steady two-dimensional incompressible laminar flow of micropolar nanofluids amid two permeable plates is taken. The base fluid is taken as blood with gold nanoparticles

suspended in it. The influence of thermal radiation, thermophoresis, and Brownian motion exists in the channel with static or moving walls. Moreover, the fluid flow is also influenced by the collective impact of chemically reactive activation energy in the presence of gyrotactic microorganisms. The geometrical view with conditions at the boundaries is presented in Figure 1. The fluid is flowing in the \hat{x} -direction, while the \hat{y} -axis is normal to the channel's walls. The walls of the channel are apart by a distance, L is the axial length, while W is the width of the channel walls. The suction and injection of flow at the walls of the channel are fixed and unvarying. Moreover, the body forces such as gravity, Coriolis, centrifugal force, and magnetic effects are ignored. At the walls, the axial velocities are assumed to be linear with the mathematical description as

$$u_{w,t} = u_t(\hat{x}/H), u_{w,b} = u_b(\hat{x}/H).$$

2.2 Mathematical description of the problem

By the suppositions in Subsection 2.1, the problem can be described mathematically as follows (Misra and Ghosh, 1997; Papadopoulos and Tzirtzilakis, 2004; Tzirtzilakis, 2005; Hatami et al., 2014; Srinivas et al., 2017):

$$\frac{\partial \hat{u}}{\partial \hat{x}} + \frac{\partial \hat{v}}{\partial \hat{y}} = 0, \tag{1}$$

$$\frac{\rho_{nf}}{\varepsilon} \left(\hat{u} \frac{\partial \hat{u}}{\partial \hat{x}} + \hat{v} \frac{\partial \hat{u}}{\partial \hat{y}} \right) = -\frac{\partial \hat{p}}{\partial \hat{x}} + (\mu_{nf} + \hat{k}) \left(\frac{\partial^2 \hat{u}}{\partial \hat{x}^2} + \frac{\partial^2 \hat{u}}{\partial \hat{y}^2} \right) + \hat{k} \frac{\partial N}{\partial \hat{y}} - \frac{\mu_{nf}}{k_1} \hat{u}, \tag{2}$$

$$\frac{\rho_{nf}}{\varepsilon} \left(\hat{u} \frac{\partial \hat{v}}{\partial \hat{x}} + \hat{v} \frac{\partial \hat{v}}{\partial \hat{y}} \right) = -\frac{\partial \hat{p}}{\partial \hat{y}} + (\mu_{nf} + \hat{k}) \left(\frac{\partial^2 \hat{v}}{\partial \hat{x}^2} + \frac{\partial^2 \hat{v}}{\partial \hat{y}^2} \right) - \hat{k} \frac{\partial N}{\partial \hat{x}} - \frac{\mu_{nf}}{k_1} \hat{v}, \tag{3}$$

$$\rho_{nf} j \left(\hat{u} \frac{\partial N}{\partial \hat{x}} + \hat{v} \frac{\partial N}{\partial \hat{y}} \right) = -k \left(2N + \frac{\partial \hat{u}}{\partial \hat{y}} - \frac{\partial \hat{v}}{\partial \hat{x}} \right) + \gamma_{nf} \left(\frac{\partial^2 N}{\partial \hat{x}^2} + \frac{\partial^2 N}{\partial \hat{y}^2} \right), \tag{4}$$

$$\hat{u} \frac{\partial T}{\partial \hat{x}} + \hat{v} \frac{\partial T}{\partial \hat{y}} = \frac{k_{nf}}{(\rho C_p)_{nf}} \left(\frac{\partial^2 T}{\partial \hat{x}^2} + \frac{\partial^2 T}{\partial \hat{y}^2} \right) - \frac{1}{(\rho C_p)_{nf}} \frac{\partial q_r}{\partial \hat{y}} + \tau \left[D_B \left(\frac{\partial C}{\partial \hat{x}} \frac{\partial T}{\partial \hat{x}} + \frac{\partial C}{\partial \hat{y}} \frac{\partial T}{\partial \hat{y}} \right) + \frac{D_T}{T_t} \left(\left(\frac{\partial T}{\partial \hat{x}} \right)^2 + \left(\frac{\partial T}{\partial \hat{y}} \right)^2 \right) \right], \tag{5}$$

$$\hat{u} \frac{\partial C}{\partial \hat{x}} + \hat{v} \frac{\partial C}{\partial \hat{y}} = D_B \left(\frac{\partial^2 C}{\partial \hat{x}^2} + \frac{\partial^2 C}{\partial \hat{y}^2} \right) + \frac{D_T}{T_t} \left(\frac{\partial^2 T}{\partial \hat{x}^2} + \frac{\partial^2 T}{\partial \hat{y}^2} \right) - k_r^2 (C - C_t) \left(\frac{T}{T_t} \right)^n \exp \left(-\frac{E_a}{k_B T} \right), \tag{6}$$

$$\hat{u} \frac{\partial n}{\partial \hat{x}} + \hat{v} \frac{\partial n}{\partial \hat{y}} + \left(\frac{bW_c}{C_b - C_t} \right) \frac{\partial}{\partial \hat{y}} \left(n \frac{\partial C}{\partial \hat{y}} \right) = D_m \frac{\partial^2 n}{\partial \hat{y}^2}. \tag{7}$$

In the aforementioned system of equations, the flow along \hat{x} , \hat{y} axes is, respectively, denoted by the components \hat{u} , \hat{v} ; \hat{p} is pressure; μ_{nf} , ρ_{nf} are dynamic viscosity and the density of the nanofluid, respectively; k_1 is permeability; ε is the porosity of walls; q_r is the heat flux due to radiation; $(\rho C_p)_{nf}$ is the effective heat capacity; k_{nf} is the thermal conductivity; D_T , D_B , D_m are diffusion coefficients for thermophoresis, Brownian motion, and microorganism, respectively; C_b , T_b , n_b are the concentration, temperature, and microorganism at the bottom plate of the channel, respectively, while C_t , T_t , n_t are the corresponding quantities at the top plate of the channel; γ_{nf} is the spine gradient viscosity which is mathematically expressed as $\gamma_{nf} = (\mu_{nf} + \hat{k}/2)j$ with j as the density of micro-inertia. Moreover, $(T/T_t)^n e^{(-E_a/k_B T)}$ is the modified Arrhenius function, E_a is the activation energy, k_r is the rate of the reaction, and W_c is the speed of microorganism cells.

The related conditions at boundaries are:

$$u(\hat{x}, \hat{y}) = u_b \frac{\hat{x}}{H}, v(\hat{x}, \hat{y}) = v_b, T = T_b, C = C_b,$$

$$n = n_b, N = -k \frac{\partial \hat{u}}{\partial \hat{y}} \text{ at } \hat{y} = 0, u(\hat{x}, \hat{y}) = u_t \frac{\hat{x}}{H},$$

$$v(\hat{x}, \hat{y}) = v_t, T = T_t, C = C_t, n = n_t, N = -k \frac{\partial \hat{u}}{\partial \hat{y}}$$

$$\text{at } \hat{y} = H. \tag{8}$$

In Eq. 8, the subscript notations b , t are used to represent the bottom and top plates of the channel, respectively. The velocities at the bottom and top walls are, respectively, denoted by v_t , v_b . It is to be noticed that these are different velocities so due to the difference in their directions, various combinations can arise. For instance, the combination $v_b > 0$, $v_t < 0$ leads to injection at the bottom and top walls. Similarly the combination $v_b < 0$, $v_t > 0$ confirms the suction at these walls (Seyf and Rassoulinejad-Mousavi, 2011). The thermophysical characteristics of gold nanoparticles are described as follows (Bachok et al., 2012; Srinivas et al., 2014; Srinivas et al., 2017):

$$\rho_{nf} = (1 - \varphi) \rho_f + \varphi \rho_s, \mu_{nf} = \frac{\mu_f}{(1 - \varphi)^{2.5}}, (\rho C_p)_{nf} = (1 - \varphi)(\rho C_p)_f + \varphi(\rho C_p)_s, \frac{k_{nf}}{k_f} = \frac{k_s + 2k_f - 2\varphi(k_f - k_s)}{k_s + 2k_f + \varphi(k_f - k_s)}. \tag{9}$$

In Eq. 9, ρ_f , k_f , $(\rho C_p)_f$ are the notations for density, thermal conductivity, and heat capacity for the base fluid, while ρ_s , k_s , $(\rho C_p)_s$ are the corresponding notations for the nanofluid. Moreover, μ_f is the viscosity of the pure fluid, while the volumetric fraction of gold nanoparticles is φ . The thermophysical characteristics of the base and nanofluids are

described numerically in Table 1 (Hatami et al., 2014; Srinivas et al., 2017):

For simplification of q_r using the Rosseland approximation as given in the following (Hatami et al., 2014; Zhang et al., 2015)

$$q_r = -\frac{4}{3} \left(\frac{\sigma^* \partial T^4}{\kappa^* \partial y} \right), \tag{10}$$

In Eq. 10, σ^* , κ^* are termed as the Stefan Boltzmann constant and the coefficient of Rosseland mean absorption such that $\sigma^* = 5.6697 \times 10^{-8} W m^{-2} K^{-4}$. If the thermal gradient is sufficiently small within the flow of the fluid, then T^4 can be simplified by using Taylor's expansion as (Zhang et al., 2015)

$$T^4 \cong 4TT_t^3 - T_t^4, \tag{11}$$

In light of Eqs. 10, 11, we have from Eq. 5 as

$$\begin{aligned} u \frac{\partial T}{\partial x} + v \frac{\partial T}{\partial y} &= \frac{k_{nf}}{(\rho C_p)_{nf}} \left(\frac{\partial^2 T}{\partial x^2} + \frac{\partial^2 T}{\partial y^2} \right) + \frac{1}{(\rho C_p)_{nf}} \left(\frac{16\sigma^* T_t^3}{3\kappa^*} \frac{\partial^2 T}{\partial y^2} \right) \\ + \tau \left[D_B \left(\frac{\partial C}{\partial x} \frac{\partial T}{\partial x} + \frac{\partial C}{\partial y} \frac{\partial T}{\partial y} \right) + \frac{D_T}{T_t} \left(\left(\frac{\partial T}{\partial x} \right)^2 + \left(\frac{\partial T}{\partial y} \right)^2 \right) \right]. \end{aligned} \tag{12}$$

The following set of variables (Srinivas et al., 2017; Shah et al., 2020; Khan et al., 2021a) will convert the leading equations into the dimensionless form:

$$\begin{aligned} x &= \frac{\hat{x}}{H}; \quad P = \frac{\hat{p}}{\rho_f v_b^2}; \quad u = \frac{\hat{u}}{v_b}; \quad v = \frac{\hat{v}}{v_b}; \quad \theta(\eta) = \frac{T - T_t}{T_b - T_t}; \\ \phi(\eta) &= \frac{C - C_t}{C_b - C_t}; \quad \chi(\eta) = \frac{n - n_t}{n_b - n_t}; \quad N = -\frac{x v_b G(\eta)}{H} \quad \text{with } \eta = \frac{y}{H}. \end{aligned} \tag{13}$$

The dimensionless velocity components are assumed as

$$u(x, \eta) = x f'(\eta); \quad v(x, \eta) = -f(\eta). \tag{14}$$

By incorporating Eqs. 13, 14 into Eqs. 1-4, 6, 7, 12, we have

$$\begin{aligned} &(1 + (1 - \varphi)^{2.5} K) f^{(iv)} - (1 - \varphi)^{2.5} K G'' - \\ &\left(1 - \varphi + \varphi \frac{\rho_s}{\rho_f} \right) (1 - \varphi)^{2.5} \text{Re} (f' f'' - f f''') - \frac{1}{Da} f'' = 0, \end{aligned} \tag{15}$$

$$\begin{aligned} &\left(1 + (1 - \varphi)^{2.5} \frac{K}{2} \right) G'' + K (1 - \varphi)^{2.5} (f'' - 2G) \\ &+ \text{Re} \left(1 - \varphi + \frac{\rho_s}{\rho_f} \varphi \right) (1 - \varphi)^{2.5} (f G' - f' G) = 0, \end{aligned} \tag{16}$$

$$\left(\frac{k_{nf}}{k_f} + \frac{4}{3} R_d \right) \theta'' + \left(1 - \varphi + \frac{(\rho C_p)_s}{(\rho C_p)_f} \right) \text{Pr} \left(\text{Re} \theta' f + N_b \theta' \phi' \right.$$

$$\left. + N_t (\theta')^2 \right) = 0, \tag{17}$$

$$\phi'' + \text{ScRe} f \phi' + \frac{N_t}{N_b} \theta'' - \text{Sc} \Gamma \phi (1 + \Omega \theta)^n \exp \left(\frac{-E}{1 + \Omega \theta} \right) = 0, \tag{18}$$

$$\chi'' - \text{Re} L_b f \chi' + \text{Pe} [\chi' \phi' + (\delta + \chi) \phi''] = 0. \tag{19}$$

In the aforementioned system of equations, $\text{Re} = v_b H / \nu_f$ is Reynolds number, $Da = k/H^2$ is the Darcy number, $\text{Pr} = (\rho C_p)_f \nu_f / k_f$ is the Prandtl number, $K = k/\mu_f$ is the material parameter, $R_d = 4\sigma^* T_t^3 / 3\kappa^* k_f$ is the radiation parameter, $N_b = \tau D_B (C_b - C_t) / \nu_f$ is the Brownian parameter, $N_t = \tau D_T (T_b - T_t) / T_t \nu_f$ is the thermophoresis parameter, $\Omega = T_b - T_t / T_t$ is the temperature parameter, $E = E_a / k_B T_t$ is the activation energy parameter, $\text{Sc} = \nu_f / D_B$ is the Schmidt number, $\Gamma = k_r^2 H^2 / \nu_f$ is the chemical reaction parameter, $L_b = \nu_f / D_m$ is the bioconvection Lewis number, $\text{Pe} = bW_c / D_m$ is the Peclet number, and $\delta = n_t / n_b - n_t$ is the microorganism concentration difference parameter.

Related conditions at boundaries are

$$\begin{aligned} f'(0) &= \lambda, \quad f(0) = -\alpha, \quad f'(1) = \gamma, \quad f(1) = -\beta, \\ \theta(0) &= 1, \quad \theta(1) = 0, \quad \phi(0) = 1, \quad \phi(1) = 0, \quad \chi(0) = 1, \\ \chi(1) &= 0, \quad G(0) = k f''(0), \quad G(1) = k f''(1). \end{aligned} \tag{20}$$

$$\text{where } \beta = \frac{v_t}{v_b}; \quad \lambda = \frac{u_t}{v_b}; \quad \gamma = \frac{u_t}{v_b}; \quad \alpha = \begin{cases} 1, & \text{for injection} \\ -1, & \text{for suction.} \end{cases} \tag{21}$$

2.3 Engineering quantities of interest

Different quantities of engineering interest for the flow system under consideration can be expressed mathematically as follows:

$$\begin{aligned} C_f &= \frac{2}{\rho_f \bar{u}^2} \left(\mu_{nf} + \bar{k} \right) \frac{\partial \bar{u}}{\partial y} \Big|_{y=0}, \quad Nu = \frac{x}{k_f (T_b - T_t)} \left(k_{nf} + \frac{16\sigma^* T_t^3}{3\kappa^*} \right) \frac{\partial T}{\partial y} \Big|_{y=0}, \\ Sh &= \frac{x}{D_B (C_b - C_t)} \left\{ -D_B \frac{\partial C}{\partial y} \Big|_{y=0} \right\}, \quad Nn = \frac{x}{D_m (n_b - n_t)} \left\{ -D_m \frac{\partial n}{\partial y} \Big|_{y=0} \right\}. \end{aligned} \tag{22}$$

Substituting Eq. 9 in Eq. 19 we have the following dimensionless quantities:

$$\begin{aligned} C_f &= \left((1 - \varphi)^{2.5} + K \right) f''(0), \quad Nu = \frac{k_{nf}}{k_f} \left(1 + \frac{4}{3} R_d \right) \theta'(0), \quad Sh \\ &= -\phi'(0), \quad Nn = -\chi'(0). \end{aligned} \tag{23}$$

3 Method for the solution

In the universe physical phenomenon, when a model give rise normally to a nonlinear mathematical model, it is very difficult and

sometimes impossible to determine the analytical solution for such a higher nonlinear mathematical model. To determine solutions to such problems, researchers have introduced different techniques. The homotopy analysis method (Liao, 1999; Liao, 2010) is one such technique that is used to solve nonlinear problems. This technique requires some initial guesses which are defined as follows:

$$\begin{aligned} \widehat{f}_0(\eta) &= (\gamma + \lambda - 2\alpha + 2\beta)\eta^3 + (3\alpha - 3\beta - 2\lambda - \gamma)\eta^2 + \lambda\eta - \alpha, \\ \widehat{G}_0(\eta) &= K(18\beta + 10\lambda + 8\gamma - 18\alpha)\eta + K(6\alpha - 6\beta - 4\lambda - 2\gamma), \\ \widehat{\Theta}_0(\eta) &= 1 - \eta, \quad \widehat{\Phi}_0(\eta) = 1 - \eta, \quad \widehat{\chi}_0(\eta) = 1 - \eta. \end{aligned} \tag{24}$$

With linear operators expressed as

$$\begin{aligned} L_f(f) &= f''' - f', \quad L_g(g) = g'' - g, \quad L_\Theta(\Theta) = \theta'' - \theta, \quad L_\Phi(\Phi) \\ &= \phi'' - \phi, \quad L_\chi(\chi) = \chi'' - \chi. \end{aligned} \tag{25}$$

In expanded form, relations in Eq. 25 can be expressed as

$$\begin{aligned} L_f(d_1 + d_2e^\eta + d_3e^{-\eta}) &= 0, \quad L_g(d_4e^\eta + d_5e^{-\eta}) = 0, \\ L_\Theta(d_6e^\eta + d_7e^{-\eta}) &= 0, \quad L_\Phi(d_8e^\eta + d_9e^{-\eta}) = 0, \\ L_\chi(d_{10}e^\eta + d_{11}e^{-\eta}) &= 0. \end{aligned} \tag{26}$$

Above d_i for $i = 1, 2, 3, \dots, 11$ are constants proceeding further as follows:

$$\begin{aligned} &N_{\widehat{f}}[\widehat{f}(\eta; \chi), \widehat{G}(\eta; \chi)\widehat{\theta}(\eta; \chi), \widehat{\phi}(\eta; \chi), \widehat{\chi}(\eta; \chi)] \\ &= (1 + (1 - \varphi)^{2.5}K)\widehat{f}_{\eta\eta\eta} + (1 - \varphi)^{2.5}K\widehat{G}_{\eta\eta} - \left(1 - \varphi \right. \\ &\quad \left. + \varphi \frac{\rho_s}{\rho_f}\right)(1 - \varphi)^{2.5}\text{Re}(\widehat{f}_\eta\widehat{f}_{\eta\eta} - \widehat{f}\widehat{f}_{\eta\eta\eta}) - \frac{1}{Da}\widehat{f}_{\eta\eta}, \end{aligned} \tag{27}$$

$$\begin{aligned} &N_{\widehat{G}}[\widehat{f}(\eta; \chi), \widehat{G}(\eta; \chi)\widehat{\theta}(\eta; \chi), \widehat{\phi}(\eta; \chi), \widehat{\chi}(\eta; \chi)] \\ &= \left(1 + (1 - \varphi)^{2.5}\frac{K}{2}\right)\widehat{G}_{\eta\eta} + K(1 - \varphi)^{2.5}(\widehat{f}_{\eta\eta} - 2\widehat{G}) \\ &\quad + \text{Re}\left(1 - \varphi + \frac{\rho_s}{\rho_f}\varphi\right)(1 - \varphi)^{2.5}(\widehat{f}\widehat{G}_\eta - \widehat{f}_\eta\widehat{G}), \end{aligned} \tag{28}$$

$$\begin{aligned} &N_{\widehat{\theta}}[\widehat{f}(\eta; \chi), \widehat{G}(\eta; \chi)\widehat{\theta}(\eta; \chi), \widehat{\phi}(\eta; \chi), \widehat{\chi}(\eta; \chi)] \\ &= \left(\frac{k_{nf}}{k_f} + \frac{4}{3}R_d\right)\widehat{\theta}_{\eta\eta} + \left(1 - \widehat{\phi} + \frac{(\rho C_p)_s}{(\rho C_p)_f}\right)\text{Pr}(\text{Re}\widehat{\theta}_\eta\widehat{f} + N_b\widehat{\theta}_\eta\widehat{\phi}_\eta \\ &\quad + N_t(\widehat{\theta}_\eta)^2), \end{aligned} \tag{29}$$

$$\begin{aligned} &N_{\widehat{\phi}}[\widehat{f}(\eta; \chi), \widehat{G}(\eta; \chi)\widehat{\theta}(\eta; \chi), \widehat{\phi}(\eta; \chi), \widehat{\chi}(\eta; \chi)] \\ &= \widehat{\phi}_{\eta\eta} + \text{ScRe}\widehat{f}\widehat{\phi}_\eta + \frac{N_t}{N_b}\theta'' - \text{Sc}\Gamma\widehat{\phi}(1 + \Omega\widehat{\theta})^n \exp\left(\frac{-E}{1 + \Omega\widehat{\theta}}\right), \end{aligned} \tag{30}$$

$$\begin{aligned} &N_{\widehat{\chi}}[\widehat{f}(\eta; \chi), \widehat{G}(\eta; \chi)\widehat{\theta}(\eta; \chi), \widehat{\phi}(\eta; \chi), \widehat{\chi}(\eta; \chi)] \\ &= \widehat{\chi}_{\eta\eta} - \text{Re}L_b\widehat{f}\widehat{\chi}_\eta + \text{Pe}[\widehat{\chi}_\eta\widehat{\phi}_\eta + (\delta + \widehat{\chi})\widehat{\phi}_{\eta\eta}]. \end{aligned} \tag{31}$$

The zero-ord/er system in respect of Eqs. 8–11 can be described as follows:

$$\begin{aligned} (1 - \zeta)L_{\widehat{f}}[\widehat{f}(\eta; \zeta) - \widehat{f}_0(\eta)] &= \zeta\widehat{h}_{\widehat{f}}N_{\widehat{f}} \\ &[\widehat{f}(\eta; \chi), \widehat{G}(\eta; \chi)\widehat{\theta}(\eta; \chi), \widehat{\phi}(\eta; \chi), \widehat{\chi}(\eta; \chi)], \end{aligned} \tag{32}$$

$$\begin{aligned} (1 - \zeta)L_{\widehat{G}}[\widehat{G}(\eta; \zeta) - \widehat{G}_0(\eta)] &= \zeta\widehat{h}_{\widehat{G}}N_{\widehat{G}} \\ &[\widehat{f}(\eta; \chi), \widehat{G}(\eta; \chi)\widehat{\theta}(\eta; \chi), \widehat{\phi}(\eta; \chi), \widehat{\chi}(\eta; \chi)], \end{aligned} \tag{33}$$

$$\begin{aligned} (1 - \zeta)L_{\widehat{\theta}}[\widehat{\theta}(\eta; \zeta) - \widehat{\theta}_0(\eta)] &= \zeta\widehat{h}_{\widehat{\theta}}N_{\widehat{\theta}} \\ &[\widehat{f}(\eta; \chi), \widehat{G}(\eta; \chi)\widehat{\theta}(\eta; \chi), \widehat{\phi}(\eta; \chi), \widehat{\chi}(\eta; \chi)], \end{aligned} \tag{34}$$

$$\begin{aligned} (1 - \zeta)L_{\widehat{\phi}}[\widehat{\phi}(\eta; \zeta) - \widehat{\phi}_0(\eta)] &= \zeta\widehat{h}_{\widehat{\phi}}N_{\widehat{\phi}} \\ &[\widehat{f}(\eta; \chi), \widehat{G}(\eta; \chi)\widehat{\theta}(\eta; \chi), \widehat{\phi}(\eta; \chi), \widehat{\chi}(\eta; \chi)], \end{aligned} \tag{35}$$

$$\begin{aligned} (1 - \zeta)L_{\widehat{\chi}}[\widehat{\chi}(\eta; \zeta) - \widehat{\chi}_0(\eta)] &= \zeta\widehat{h}_{\widehat{\chi}}N_{\widehat{\chi}} \\ &[\widehat{f}(\eta; \chi), \widehat{G}(\eta; \chi)\widehat{\theta}(\eta; \chi), \widehat{\phi}(\eta; \chi), \widehat{\chi}(\eta; \chi)]. \end{aligned} \tag{36}$$

The BCs are

$$\begin{aligned} \left.\frac{\partial \widehat{f}(\eta; \zeta)}{\partial \eta}\right|_{\eta=0} &= \lambda, \quad \left.\frac{\partial \widehat{f}(\eta; \zeta)}{\partial \eta}\right|_{\eta=1} = \gamma, \quad \widehat{f}(\eta; \zeta)\Big|_{\eta=0} = -\alpha, \quad \widehat{f}(\eta; \zeta)\Big|_{\eta=1} \\ &= -\beta, \quad \widehat{\theta}(\eta; \zeta)\Big|_{\eta=0} = 1, \quad \widehat{\theta}(\eta; \zeta)\Big|_{\eta=1} = 0, \quad \widehat{\phi}(\eta; \zeta)\Big|_{\eta=0} = 1, \quad \widehat{\phi}(\eta; \zeta)\Big|_{\eta=1} \\ &= 0, \quad \widehat{\chi}(\eta; \zeta)\Big|_{\eta=0} = 1, \quad \widehat{\chi}(\eta; \zeta)\Big|_{\eta=1} = 0, \quad \widehat{G}(\eta; \zeta)\Big|_{\eta=0} \\ &= k\frac{\partial^2 \widehat{f}(\eta; \zeta)}{\partial \eta^2}\Big|_{\eta=0}, \quad \widehat{G}(\eta; \zeta)\Big|_{\eta=1} = k\frac{\partial^2 \widehat{f}(\eta; \zeta)}{\partial \eta^2}\Big|_{\eta=1}. \end{aligned} \tag{37}$$

It is to be noticed that $\zeta \in [0, 1]$, so for $\zeta = 0$ and $\zeta = 1$ we have

$$\begin{aligned} \widehat{f}(\eta; 1) &= \widehat{f}(\eta), \quad \widehat{G}(\eta; 1) = \widehat{G}(\eta), \quad \widehat{\theta}(\eta; 1) = \widehat{\theta}(\eta), \quad \widehat{\phi}(\eta; 1) \\ &= \widehat{\phi}(\eta), \quad \widehat{\chi}(\eta; 1) = \widehat{\chi}(\eta). \end{aligned} \tag{38}$$

The expansion of Taylor's series for $\widehat{f}(\eta; \zeta)$, $\widehat{G}(\eta; \zeta)$, $\widehat{\theta}(\eta; \zeta)$, $\widehat{\phi}(\eta; \zeta)$, and $\widehat{\chi}(\eta; \zeta)$ around $\zeta = 0$

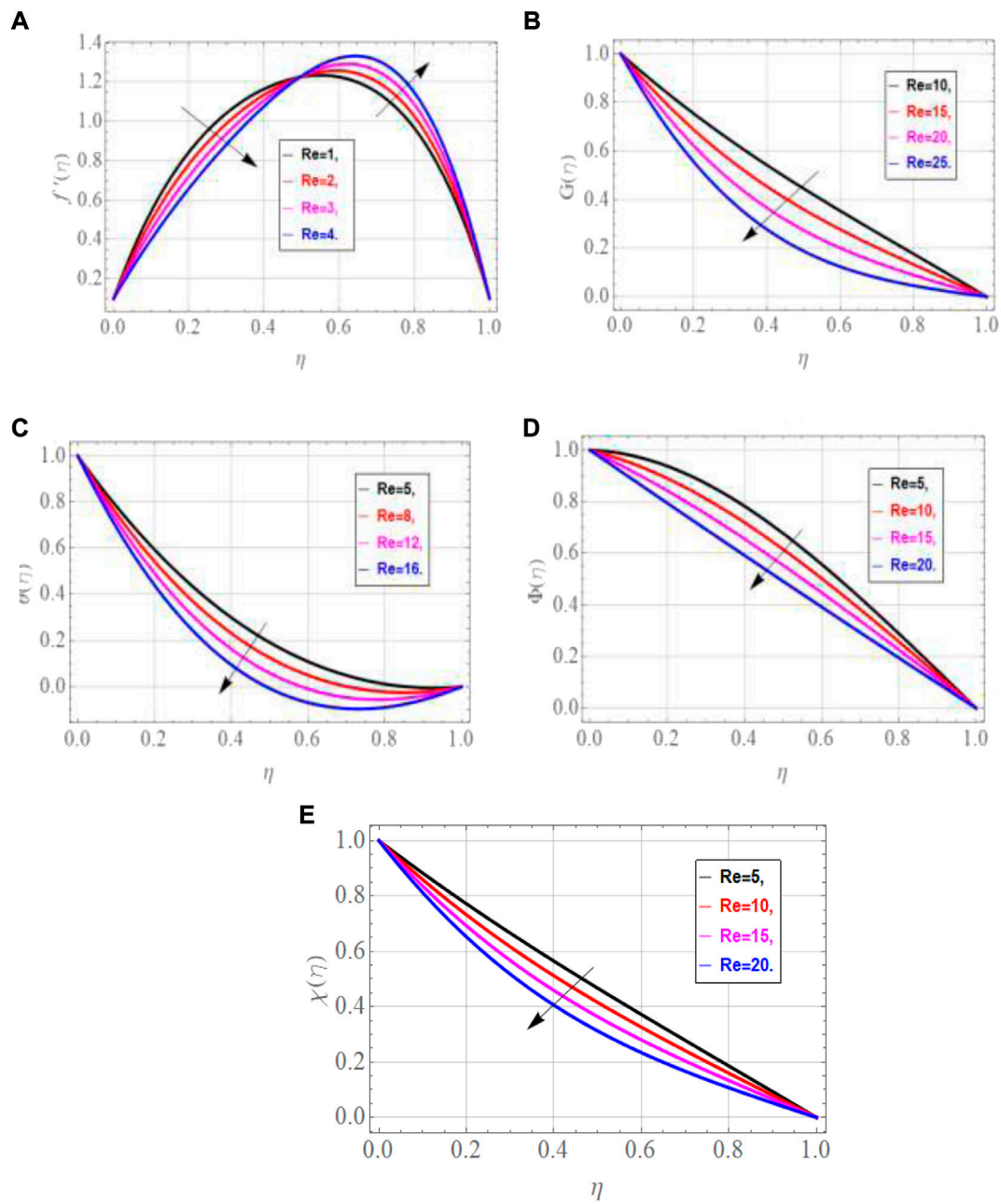


FIGURE 2 Impact of Re on $f'(\eta)$, $G(\eta)$, $\theta(\eta)$, $\Phi(\eta)$, $\chi(\eta)$.

$$\begin{aligned}
 \widehat{f}(\eta; \zeta) &= \widehat{f}_0(\eta) + \sum_{n=1}^{\infty} \widehat{f}_n(\eta) \zeta^n, \\
 \widehat{G}(\eta; \zeta) &= \widehat{G}_0(\eta) + \sum_{n=1}^{\infty} \widehat{G}_n(\eta) \zeta^n, \\
 \widehat{\theta}(\eta; \zeta) &= \widehat{\theta}_0(\eta) + \sum_{n=1}^{\infty} \widehat{\theta}_n(\eta) \zeta^n, \\
 \widehat{\phi}(\eta; \zeta) &= \widehat{\phi}_0(\eta) + \sum_{n=1}^{\infty} \widehat{\phi}_n(\eta) \zeta^n, \\
 \widehat{\chi}(\eta; \zeta) &= \widehat{\chi}_0(\eta) + \sum_{n=1}^{\infty} \widehat{\chi}_n(\eta) \zeta^n,
 \end{aligned}
 \tag{39}$$

$$\begin{aligned}
 \widehat{f}_n(\eta) &= \frac{1}{n!} \left. \frac{\partial \widehat{f}(\eta; \zeta)}{\partial \zeta} \right|_{\zeta=0}, \quad \widehat{G}_n(\eta) = \frac{1}{n!} \left. \frac{\partial \widehat{G}(\eta; \zeta)}{\partial \zeta} \right|_{\zeta=0}, \quad \widehat{\theta}_n(\eta) \\
 &= \frac{1}{n!} \left. \frac{\partial \widehat{\theta}(\eta; \zeta)}{\partial \zeta} \right|_{\zeta=0}, \quad \widehat{\phi}_n(\eta) = \frac{1}{n!} \left. \frac{\partial \widehat{\phi}(\eta; \zeta)}{\partial \zeta} \right|_{\zeta=0}, \quad \widehat{\chi}_n(\eta) = \frac{1}{n!} \left. \frac{\partial \widehat{\chi}(\eta; \zeta)}{\partial \zeta} \right|_{\zeta=0}.
 \end{aligned}
 \tag{40}$$

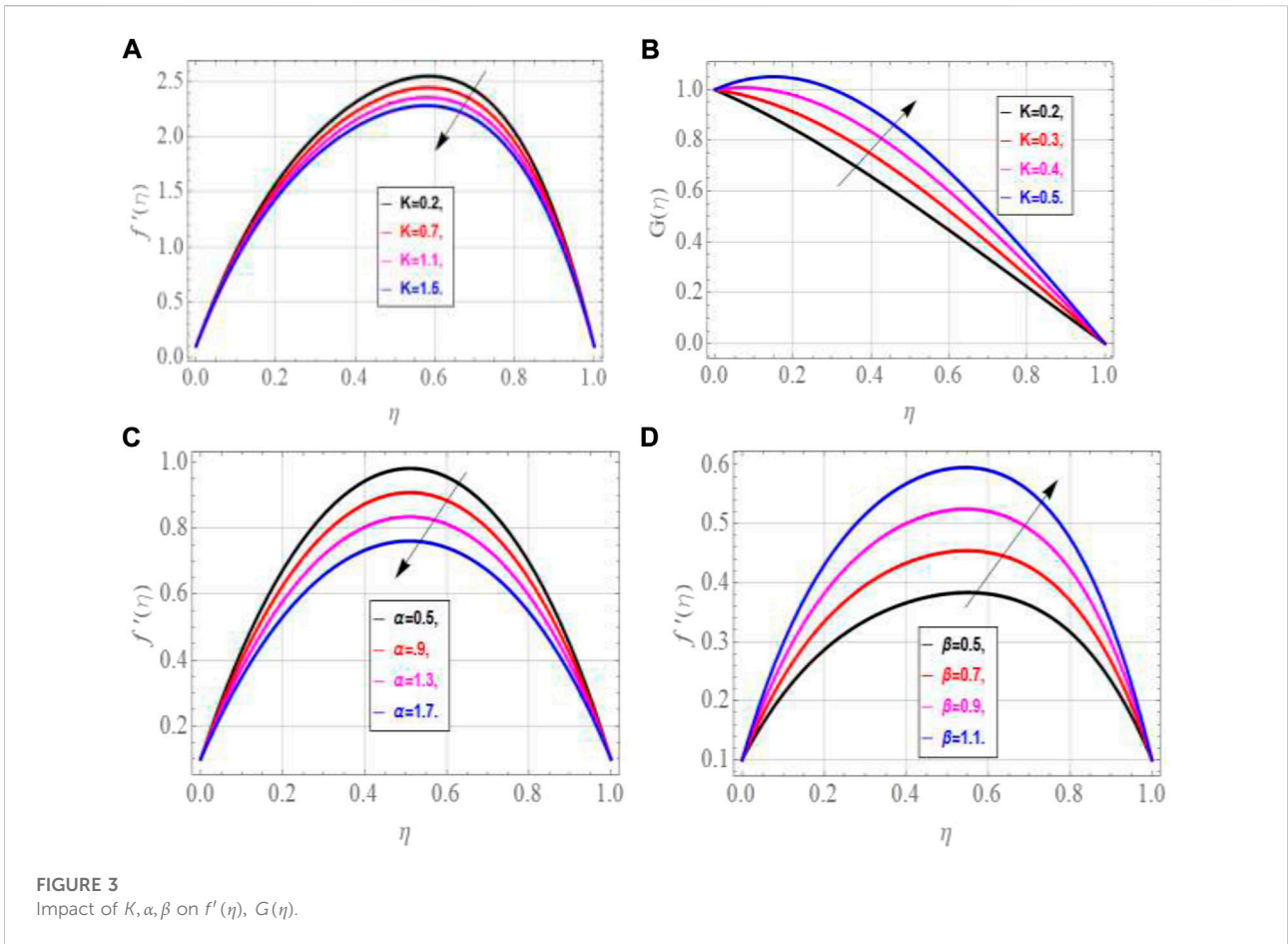


FIGURE 3 Impact of K, α, β on $f'(\eta), G(\eta)$.

With boundary conditions as follows

$$-f'(0) = \lambda, -f'(1) = \gamma, \hat{f}(0) = -\alpha, \hat{f}(1) = -\beta, \hat{G}(0) =$$

$$= k - f''(0), \hat{G}(1)$$

$$= k - f''(1), \hat{\theta}(0) = 1, \hat{\theta}(1) = 0, \quad (41)$$

$$\hat{\phi}(0) = 1, \hat{\phi}(1) = 0, \hat{\chi}(0) = 1, \hat{\chi}(1) = 0.$$

Next, we have

$$\Re_n \hat{f}(\eta) = (1 + (1 - \varphi)^{2.5} K) \hat{f}_{n-1}^{iv} + (1 - \varphi)^{2.5} K \hat{G}_{n-1}'' - \left(1 - \varphi + \varphi \frac{\rho_s}{\rho_f}\right) (1 - \varphi)^{2.5} \text{Re} \left(\hat{f}_{n-1}'' \sum_{j=0}^{w-1} \hat{f}_{w-1-j} \hat{f}_j'' \right) - \frac{1}{Da} \hat{f}_{n-1}'' \quad (42)$$

$$\Re_n \hat{G}(\eta) = \left(1 + (1 - \varphi)^{2.5} \frac{K}{2}\right) \hat{G}_{n-1}'' + K(1 - \varphi)^{2.5} \sum_{j=0}^{w-1} (\hat{f}_{n-1}'' \hat{G}_{w-1-j}) + \text{Re} \left(1 - \varphi + \frac{\rho_s}{\rho_f} \varphi\right) (1 - \varphi)^{2.5} \sum_{j=0}^{w-1} (\hat{f}_{w-1-j} \hat{G}_{n-1}'' \hat{f}_{n-1}'' \hat{G}_{w-1-j}), \quad (43)$$

$$\Re_n \hat{\theta}(\eta) = \left(\frac{k_{nf}}{k_f} + \frac{4}{3} R_d\right) \hat{\theta}_{n-1}'' \left(1 - \hat{\phi} + \frac{(\rho C_p)_s}{(\rho C_p)_f}\right)$$

$$\text{Pr} \left(\text{Re} \sum_{j=0}^{w-1} \hat{\theta}_{n-1}'' f_{w-1-j} + N_b \hat{\theta}_{n-1}'' \phi_{n-1}' + N_t (\hat{\theta}_{n-1}'')^2 \right), \quad (44)$$

$$\Re_n \hat{\phi}(\eta) = \hat{\phi}_{n-1}'' + \text{Sc} \text{Re} \hat{f} \hat{\phi}_{n-1}' + \frac{N_t}{N_b} \hat{\theta}_{n-1}'' - \text{Sc} \Gamma (1 + \Omega \hat{\theta})'' \exp\left(\frac{-E}{1 + \Omega \hat{\theta}}\right) \sum_{j=0}^{w-1} \phi_{w-1-j}, \quad (45)$$

$$\Re_n \hat{\chi}(\eta) = \hat{\chi}_{n-1}'' \text{Re} \sum_{j=0}^{w-1} L_b \hat{f}_j \hat{\chi}_{w-1-j} \text{Pr} e \left(\sum_{j=0}^{w-1} \hat{\chi}_{w-1-j} \hat{\phi}_j + \sum_{j=0}^{w-1} (\delta + \hat{\chi}_{w-1-j}) \hat{\phi}_{n-1}'' \right). \quad (46)$$

Moreover, we have

$$\xi_n = \begin{cases} 0, & \text{if } \zeta \leq 1 \\ 1, & \text{if } \zeta > 1. \end{cases} \quad (47)$$

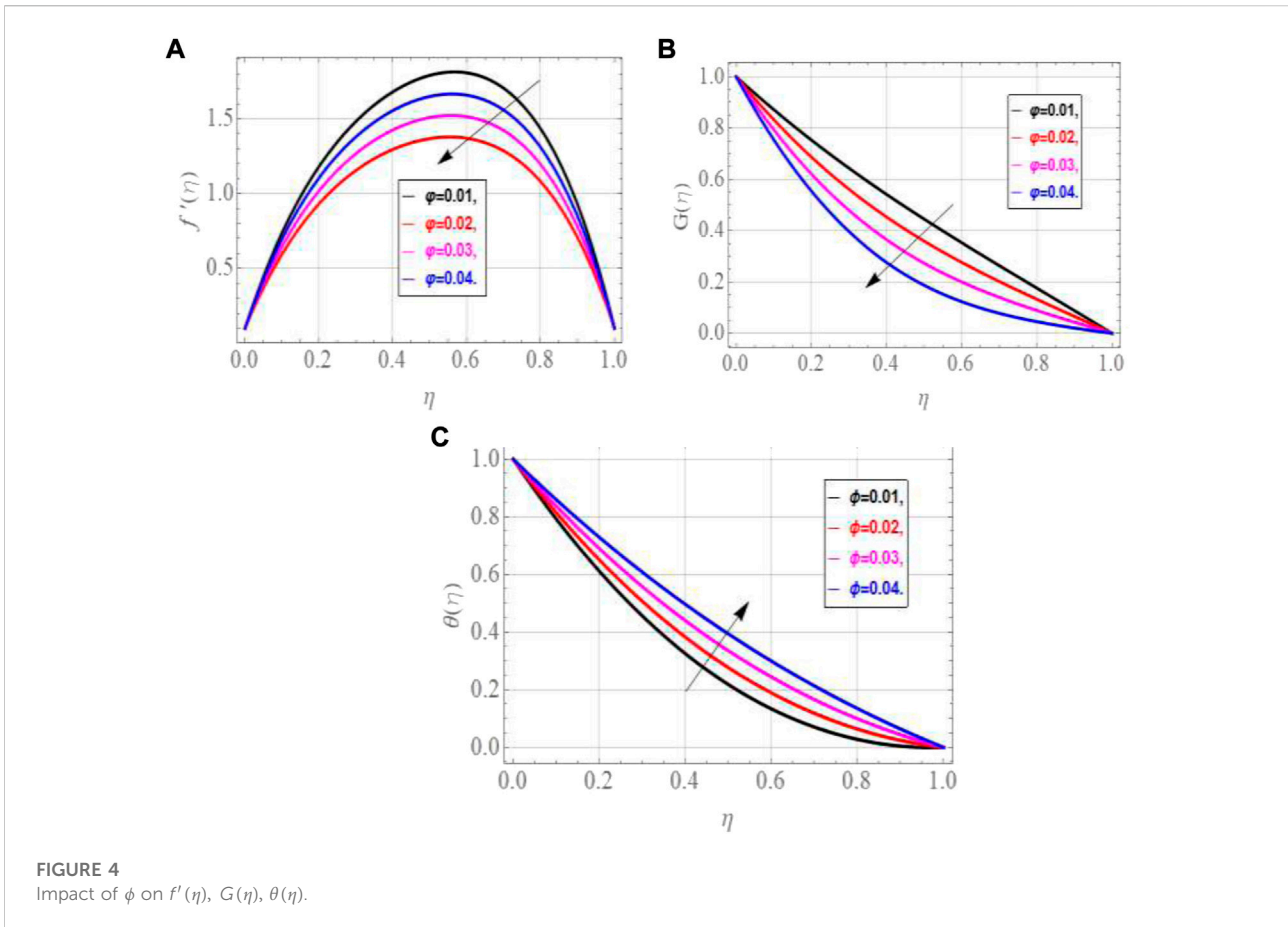


FIGURE 4 Impact of ϕ on $f'(\eta)$, $G(\eta)$, $\theta(\eta)$.

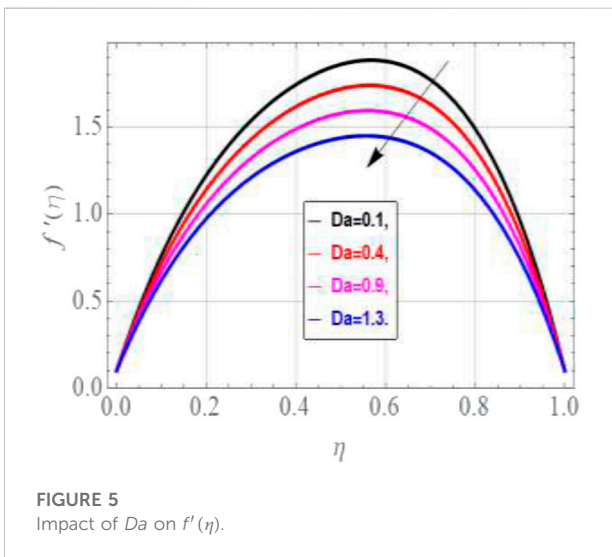


FIGURE 5 Impact of Da on $f'(\eta)$.

4 Discussion of results

The current study examines the flow and heat transfer for the flow of blood that comprises micropolar gold

nanoparticles. The influence of chemically reactive activation energy, thermophoresis, thermal radiations, and Brownian motion also exists between the walls of the channel. A microorganism creation also affects the concentration of nanoparticles inside the channel. Suitable transformation has been used to change the mathematical model to the dimensionless form and then has been solved by employing the homotopy analysis method. The impact upon different profiles of flow systems in response to variations in the physical parameter has been comprehended in the following.

Figure 2 depicts the influence of the Reynolds number Re on different profiles of the flow system. Since the Reynolds number signifies the comparison of inertial force to viscous force, so augmentation in Re causes domination of inertial to viscous force. This physical phenomenon declines the rotational flow, thermal characteristics, motility, and concentration of micropolar nanoparticles. In the case of linear velocity, the flow behavior is two-folded over the range $0 \leq \eta \leq 1$. The flow is declining in the range $0 \leq \eta \leq 0.5$, whereas it is augmenting on the range $0.5 \leq \eta \leq 1$.

Figure 3 describes the changing behavior of fluid's motion for variation in the values of the material parameter. From

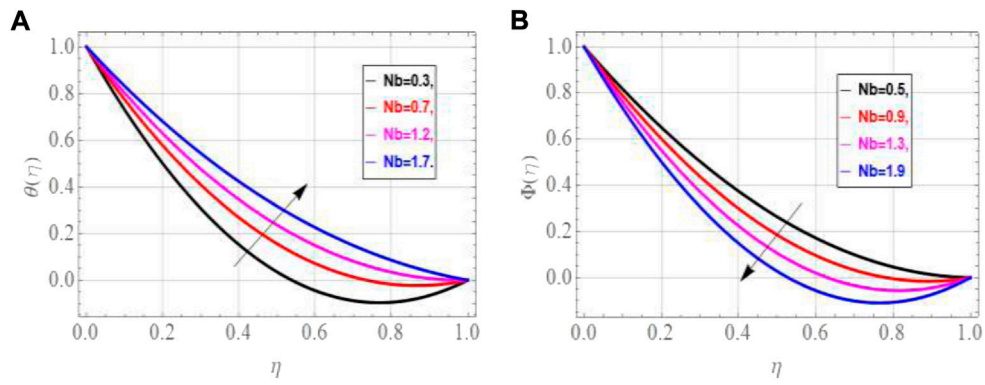


FIGURE 6
Impact of Nb on $\theta(\eta)$, $\Phi(\eta)$.

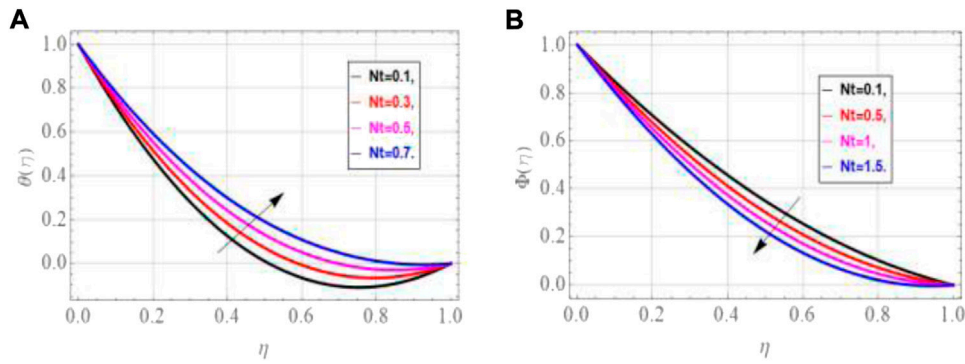


FIGURE 7
Impact of Nt on $\theta(\eta)$, $\Phi(\eta)$.

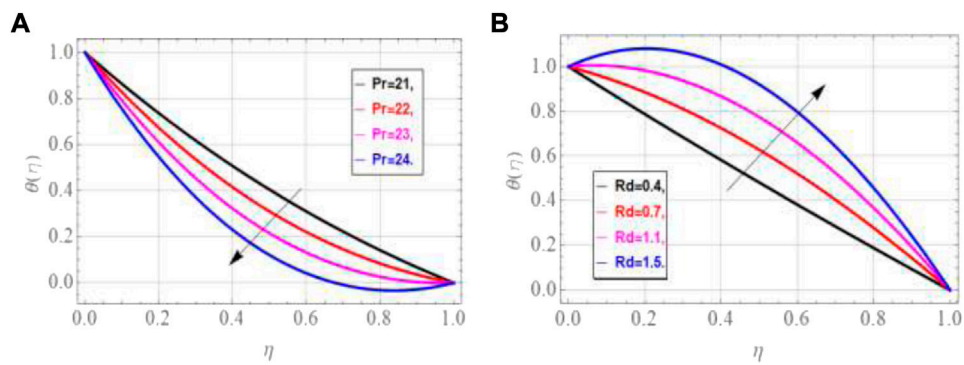


FIGURE 8
Impact of Pr and Rd on $\theta(\eta)$.

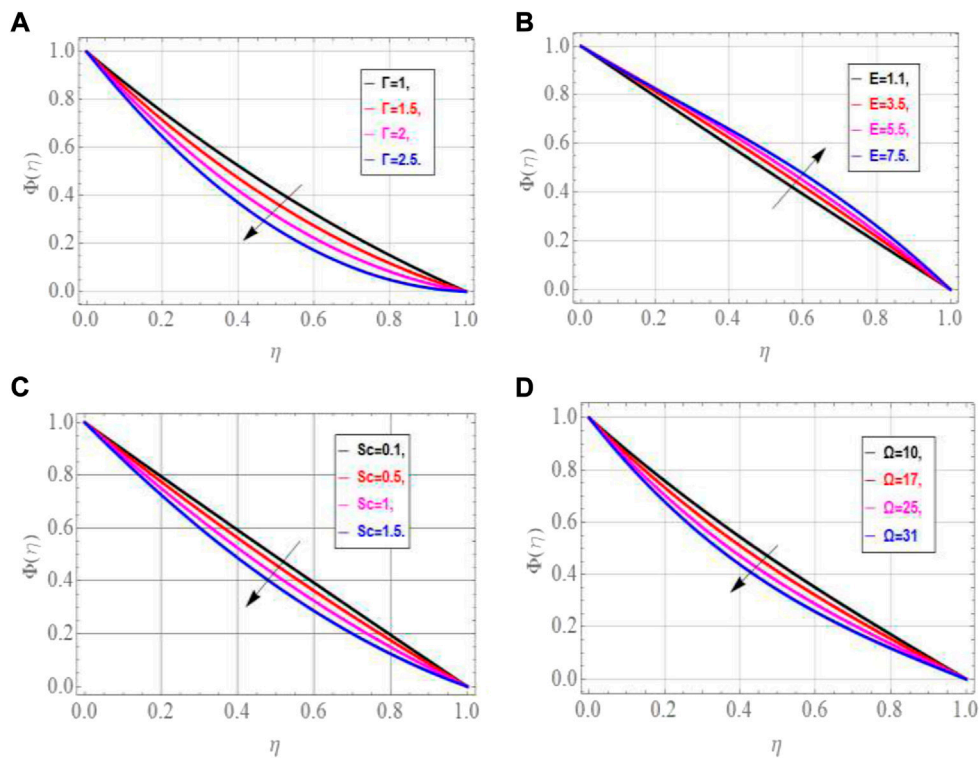


FIGURE 9
Impact of Γ , E , Sc and Ω on $\Phi(\eta)$.

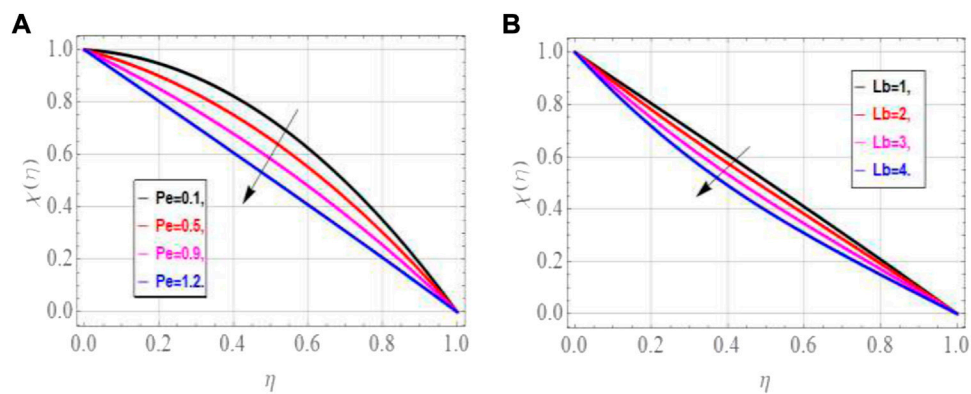


FIGURE 10
Impact of Pe , Lb on $\chi(\eta)$.

Figure 3A, it can be perceived that fluid's motion declines in the closed locality of the porous plate with augmentation in K due to domination of vertex viscosity to dynamic viscosity. In this physical process, the rotational effects are enhanced in the fluid particles that cause augmentation in the microrotation

flow of nanofluids, as depicted in Figure 3B. It has also been noticed that the flow profiles have declined with augmentation in the suction parameter, as depicted in Figure 3C. Moreover, augmenting values of the injection parameter have supported the velocity, as depicted in Figure 3D.

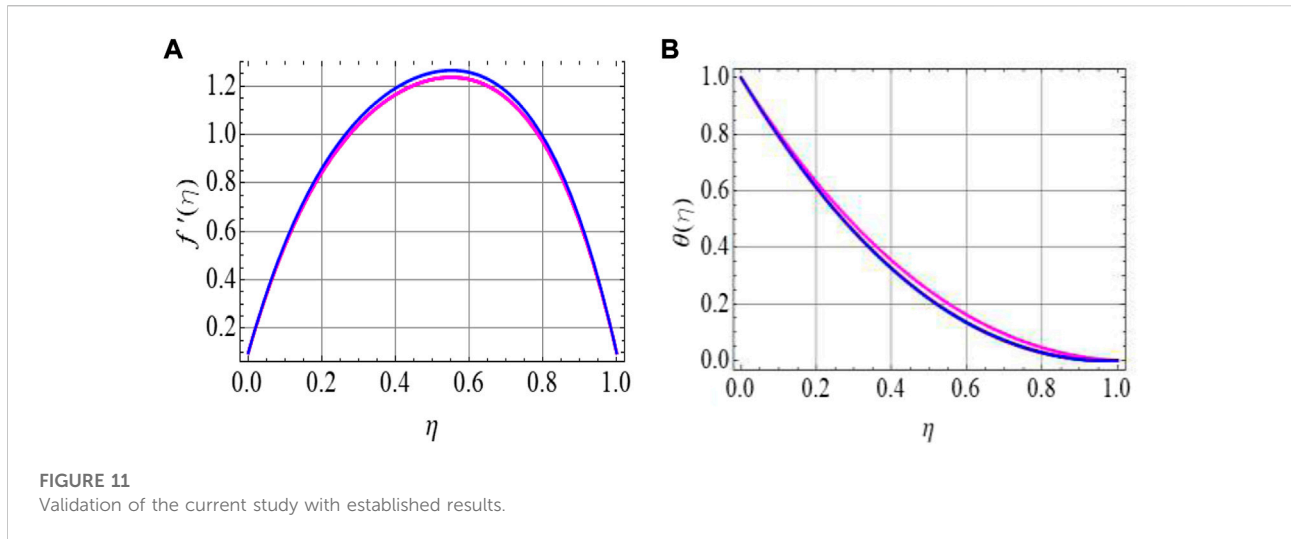


TABLE 1 Thermophysical properties of the base fluid and nanoparticles.

| Material | Density (kg/m^3) | Specific heat (J/kgK) | Thermal conductivity (W/mK) |
|----------|----------------------|---------------------------|---------------------------------|
| Blood | 1,050 | 3,617 | 0.52 |
| Gold | 19,300 | 129 | 318 |

TABLE 2 Skin friction C_f variations for different values of Re and Da .

| ϕ | K | Re | Da | $f'(1)$ | $f'(0)$ |
|--------|-----|------|------|---------|-----------|
| 0.02 | 0.3 | 1 | 0.5 | 6.1963 | -0.15248 |
| 0.04 | | | | 6.98229 | -0.21329 |
| 0.06 | | | | 7.87492 | -0.27577 |
| 0.02 | | 1 | 1 | 6.19630 | -0.15248 |
| | | | | 5.94500 | -0.13451 |
| | | | | 5.14270 | -0.08936 |
| 0.04 | | 1 | 3 | 6.19630 | -0.15248 |
| | | | | 6.71085 | -0.210436 |
| | | | | 7.30327 | -0.295691 |
| 0.06 | | 1 | 5 | 6.19630 | -0.152480 |
| | | | | 6.49150 | -0.249460 |
| | | | | 6.97020 | -0.305632 |

TABLE 3 Nusselt number Nu for variations Nb and Rd .

| Nt | Nb | Rd | $\theta'(1)$ | $\theta'(0)$ |
|------|------|------|--------------|--------------|
| 0.2 | 0.5 | 0.5 | 5.29822 | -0.73111 |
| | | | 6.06530 | -0.80198 |
| | | | 6.28720 | -0.84279 |
| 0.4 | 0.5 | 0.5 | 5.29822 | -0.73111 |
| | | | 6.10851 | -0.74766 |
| | | | 6.33041 | -0.78847 |
| 0.6 | 0.5 | 0.5 | 5.29822 | -0.73111 |
| | | | 6.07098 | -0.70144 |
| | | | 6.29288 | -0.74225 |

Figure 4 depicts the impact of volumetric fraction ϕ on the flow, microrotational flow, and thermal profiles of the micropolar nanofluid. Since the augmenting values of ϕ cause an enhancement in the viscous forces amongst the fluid nanoparticles, the fluid becomes more dense and viscous. During this process, higher resistance is experienced by micropolar nanoparticles that decline the fluid flow in all

directions, as shown in Figures 4A,B, while augmenting the thermal profiles of micropolar nanofluids, as depicted in Figure 4C.

Figure 5 portrays that augmenting values in the Darcy number Da decay the flow profiles. Actually, the void spaces in the porous plates are augmented with growing values of Da that offer more confrontation to the fluid's flow and decline the flow profile.

Figure 6 reveals that augmentation in Nb supports the thermal profile and opposes the mass flow of the micropolar

TABLE 4 Sherwood number Sh variation for different values of Nb and Rd .

| Nt | Nb | Re | Sc | $\phi'(1)$ | $\phi'(0)$ |
|------|------|------|------|------------|------------|
| 0.2 | 0.5 | 0.5 | | 0.314193 | -3.49654 |
| 0.4 | | | | 0.3702185 | -3.56741 |
| 0.6 | | | | 0.4208461 | -3.60822 |
| | 0.5 | | | 0.314193 | -3.49654 |
| | 0.8 | | | 0.2764301 | -3.07410 |
| | 1.1 | | | 0.2064107 | -2.49630 |
| | | 0.35 | | 0.314193 | -3.49654 |
| | | 1 | | 0.4864106 | -4.17539 |
| | | 1.5 | | 0.5475302 | -4.932865 |
| | | | 0.3 | 0.314193 | -3.49654 |
| | | | 0.5 | 0.2953106 | -3.18640 |
| | | | 0.7 | 0.2507270 | -2.70871 |

nanofluid. Physically an enhancement in Nb causes an increment in the collision amongst the nanoparticles due to their random motion between the porous plates. In this process, kinetic energy amongst the particles is transformed to thermal energy and causes less transfer of the mass of the fluid. Hence, the thermal profiles enhance and the concentration of fluid declines for augmenting values of Nb .

Figure 7 depicts the influence of the thermophoresis parameter Nt on (η) , $\Phi(\eta)$. Actually, augmentation in Nt corresponds to more thermal and less mass diffusivity of the micropolar nanofluid. Hence, the thermal characteristics increase, and the mass flow declines with augmenting values of Nt .

Figure 8 depicts the impact of the Prandtl number Pr and radiation parameter Rd upon thermal profiles. Figure 8A reveals a significant decline in thermal profiles. Actually, Pr is inversely proportional to heat diffusion due to which the thermal profiles decline for augmenting values of Pr . Figure 8B shows that for enhancing values of Rd , more heat transfer takes place that augments the thermal profiles.

Figure 9 portrays the variations in concentration in response to the chemical reaction parameter Γ , dimensionless activation energy parameter E , Schmidt number Sc , and temperature ratio parameter Ω . For augmentation in Γ , the molecules of the micropolar fluid diffuse slowly due to which less mass diffusion occurs and decays the concentration, as depicted in Figure 9A. For greater values of E , the bulk of molecules that requires less energy supports maximum transmission of mass. Hence, greater values of E cause growth in the concentration of micropolar nanoparticles, as depicted in Figure 9B. For augmenting values of Sc , less mass transfer takes place which weakens the strength of the concentration layer and decays the concentration profiles, as portrayed in Figure 9C. The difference in temperature enhances growth in Ω and causes maximum transmission of heat at the free

stream. In this physical process, less mass diffuses which causes a decline in the concentration, as shown in Figure 9D.

Figure 10 depicts the effects of Peclet and bioconvection Lewis numbers Pe , Lb on the density number of motile microorganisms. It has been noticed from this figure that the growth in Pe , Lb causes a decline in the spread of microorganisms that weakens the strength of its boundary layer. Hence, the growing values of Pe , Lb decline the density number of microorganisms.

Figures 11A,B present the validation of the current investigation. In this figure, the present results are validated with published studies given in Shah et al. (2019) by considering the common parameters. This figure shows a close agreement between the present results and published studies.

4.1 Table discussion

The influence upon various physical quantities in response to different emerging parameters has been presented numerically in Table 1. The numerical results of the velocity gradient C_f against different emerging parameters are given in Table 2. One can find that the velocity gradient upsurges for the particle concentration, Reynolds number Re , and Darcy number. Prominent performances of various engineering parameters on the Nusselt number Nu are examined in Table 3. As expected, the Nusselt number is augmented for expansion in the thermophoresis parameter, Brownian parameter Nb , and radiation parameter Rd . The characteristics of Nb and Re on the Sherwood number Sh are scrutinized in Table 4. One can clearly notice that the concentration gradient is augmented for a higher approximation of Re , while declines with Nb and Sc .

5 Conclusion

In this investigation, the flow and heat transfer for the flow of blood comprises micropolar gold nanoparticles. The influence of chemically reactive activation energy, thermophoresis, thermal radiations, and Brownian motion exists between the walls of the channel. A microorganism creation also affects the concentration of nanoparticles inside the channel. The impact on different profiles of flow systems in response to variations in the physical parameter has been discussed graphically. After a detailed inspection of the research, some main points have been noted and appended in the following:

- Reynolds number reduces all the profiles of the flow system.
- The augmentation in the material parameter and Darcy number declines the flow of the fluid and upsurges the microrotation velocity of nanoparticles.
- The augmenting values of the volumetric fraction cause an enhancement in viscous forces amongst the fluid

nanoparticles and cause a reduction in the flow of the fluid in all direction while supporting the thermal profiles.

- Thermal profiles are supported while concentration profiles are opposed by the growing values of thermophoresis and the Brownian motion parameter.
- Thermal profiles are also growing up with augmenting values of the radiation parameter and decline with enhancement in the Prandtl number.
- The concentration of fluid upsurges by higher values of the activation energy parameter and reduces by growth in the chemical reaction parameter, Schmidt number, and temperature ratio parameter.
- An augmentation in the bioconvection Lewis number and Peclet number opposes the growth in motile microorganisms.

Data availability statement

The original contributions presented in the study are included in the article/supplementary material; further inquiries can be directed to the corresponding author.

Author contributions

AK has modeled the problem. Dr. Safyan Mukhtar has solved the modeled problem by HAM. AK and WA wrote the manuscript. Dr. Safyan Mukhtar and AK have also contributed to the numerical computations and plotting of the graphical results of the manuscript. MA, MMA,

MPFY, ET participated in revision of manuscript. All the authors have finalized the manuscript after its internal evaluation.

Acknowledgments

“The authors extend their appreciation to the Deanship of Scientific Research at King Khalid University for funding this work through Large Groups” [Project under grant number (RGP.2/116/43)].

Conflict of interest

The authors declare that the research was conducted in the absence of any commercial or financial relationships that could be construed as a potential conflict of interest.

Publisher's note

All claims expressed in this article are solely those of the authors and do not necessarily represent those of their affiliated organizations, or those of the publisher, the editors, and the reviewers. Any product that may be evaluated in this article, or claim that may be made by its manufacturer, is not guaranteed or endorsed by the publisher.

References

- Abbas, N., Nadeem, S., and Malik, M. Y. (2020). Theoretical study of micropolar hybrid nanofluid over Riga channel with slip conditions. *Phys. A Stat. Mech. Its Appl.* 551, 124083. doi:10.1016/j.physa.2019.124083
- Ahmad, S., Ashraf, M., and Ali, K. (2020). Nanofluid flow comprising gyrotactic microorganisms through a porous medium. *J. Appl. Fluid Mech.* 13 (5), 1539–1549. doi:10.36884/jafm.13.05.31030
- Ayub, A., Darvesh, A., Altamirano, G. C., and Sabir, Z. (2021). Nanoscale energy transport of inclined magnetized 3D hybrid nanofluid with Lobatto IIIA scheme. *Heat. Transf.* 50 (7), 6465–6490. doi:10.1002/htj.22188
- Ayub, A., Sabir, Z., Le, D. N., and Aly, A. A. (2021). Nanoscale heat and mass transport of magnetized 3-D chemically radiative hybrid nanofluid with orthogonal/inclined magnetic field along rotating sheet. *Case Stud. Therm. Eng.* 26, 101193. doi:10.1016/j.csite.2021.101193
- Ayub, A., Sabir, Z., Shah, S. Z. H., Mahmoud, S. R., Algarni, A., Sadat, R., et al. (2022b). Aspects of infinite shear rate viscosity and heat transport of magnetized Carreau nanofluid. *Eur. Phys. J. Plus* 137 (2), 1–25. doi:10.1140/epjp/s13360-022-02410-6
- Ayub, A., Sabir, Z., Shah, S. Z. H., Wahab, H. A., Sadat, R., and Ali, M. R. (2022c). Effects of homogeneous-heterogeneous and Lorentz forces on 3-D radiative magnetized cross nanofluid using two rotating disks. *Int. Commun. Heat Mass Transf.* 130, 105778. doi:10.1016/j.icheatmasstransfer.2021.105778
- Ayub, A., Shah, S. Z. H., Sabir, Z., Rao, N. S., Sadat, R., and Ali, M. R. (2022). Spectral relaxation approach and velocity slip stagnation point flow of inclined magnetized cross-nanofluid with a quadratic multiple regression model. *Waves Random Complex Media* 107, 1–25. doi:10.1080/17455030.2022.2049923
- Ayub, A., Wahab, H. A., Shah, S. Z., Shah, S. L., Darvesh, A., Haider, A., et al. (2021). Interpretation of infinite shear rate viscosity and a nonuniform heat sink/source on a 3D radiative cross nanofluid with buoyancy assisting/opposing flow. *Heat. Transf.* 50 (5), 4192–4232. doi:10.1002/htj.22071
- Bachok, N., Ishak, A., and Pop, I. (2012). The boundary layers of an unsteady stagnation-point flow in a nanofluid. *Int. J. Heat Mass Transf.* 55 (23–24), 6499–6505. doi:10.1016/j.ijheatmasstransfer.2012.06.050
- Baharifarid, F., Parand, K., and Rashidi, M. M. (2020). Novel solution for heat and mass transfer of a MHD micropolar fluid flow on a moving plate with suction and injection. *Eng. Comput.* 38, 13–30. doi:10.1007/s00366-020-01026-7
- Bin-Mohsin, B., Ahmed, N., Khan, U., Mohyud-Din, S. T., and Tauseef Mohyud-Din, S. (2017). A bioconvection model for a squeezing flow of nanofluid between parallel plates in the presence of gyrotactic microorganisms. *Eur. Phys. J. Plus* 132 (4), 1–12. doi:10.1140/epjp/i2017-11454-4
- Choi, S. U., and Eastman, J. A. (1995). Enhancing thermal conductivity of fluids with nanoparticles. *ASME Fluids Eng. Div.* 231, 99–105.
- Delhi Babu, R., and Ganesh, S. (2020). The mathematical model for steady magnetohydrodynamic flow between parallel porous plates with an angular velocity. *Int. J. Ambient Energy* 41 (11), 1284–1292. doi:10.1080/01430750.2018.1507944
- Eringen, A. C. (1966). Theory of micropolar fluids. *Indiana Univ. Math. J.* 16, 1–18. doi:10.1512/iumj.1967.16.16001
- Fakour, M., Vahabzadeh, A., Ganji, D. D., and Hatami, M. (2015). Analytical study of micropolar fluid flow and heat transfer in a channel with permeable walls. *J. Mol. Liq.* 204, 198–204. doi:10.1016/j.molliq.2015.01.040

- Hassan, A. R. (2020). The entropy generation analysis of a reactive hydromagnetic couple stress fluid flow through a saturated porous channel. *Appl. Math. Comput.* 369, 124843. doi:10.1016/j.amc.2019.124843
- Hatami, M., Hatami, J., and Ganji, D. D. (2014). Computer simulation of MHD blood conveying gold nanoparticles as a third grade non-Newtonian nanofluid in a hollow porous vessel. *Comput. methods programs Biomed.* 113 (2), 632–641. doi:10.1016/j.cmpb.2013.11.001
- Islam, S., Khan, A., Deebani, W., Bonyah, E., Alreshidi, N. A., and Shah, Z. (2020). Influences of Hall current and radiation on MHD micropolar non-Newtonian hybrid nanofluid flow between two surfaces. *AIP Adv.* 10 (5), 055015. doi:10.1063/1.5145298
- Khan, A., Saeed, A., Tassaddiq, A., Gul, T., Kumam, P., Ali, I., et al. (2021). Bio-convective and chemically reactive hybrid nanofluid flow upon a thin stirring needle with viscous dissipation. *Sci. Rep.* 11 (1), 1–17. doi:10.1038/s41598-021-86968-8
- Khan, A., Saeed, A., Tassaddiq, A., Gul, T., Mukhtar, S., Kumam, P., et al. (2021). Bio-convective micropolar nanofluid flow over thin moving needle subject to Arrhenius activation energy, viscous dissipation and binary chemical reaction. *Case Stud. Therm. Eng.* 25, 100989. doi:10.1016/j.csite.2021.100989
- Liao, S. J. (1999). An explicit, totally analytic approximate solution for Blasius' viscous flow problems. *Int. J. Non. Linear. Mech.* 34, 759–778. doi:10.1016/s0020-7462(98)00056-0
- Liao, S. J. (2010). An optimal homotopyanalysis approach for strongly nonlinear differential equations. *Commun. Nonlinear Sci. Numer. Simul.* 15, 2003–2016. doi:10.1016/j.cnsns.2009.09.002
- Misra, J. C., and Ghosh, S. K. (1997). A mathematical model for the study of blood flow through a channel with permeable walls. *Acta Mech.* 122 (1), 137–153. doi:10.1007/bf01181995
- Papadopoulos, P. K., and Tzirtzilakis, E. E. (2004). Biomagnetic flow in a curved square duct under the influence of an applied magnetic field. *Phys. Fluids* 16 (8), 2952–2962. doi:10.1063/1.1764509
- Platt, J. R. (1961). Bioconvection patterns in cultures of free-swimming organisms. *Science* 133 (3466), 1766–1767. doi:10.1126/science.133.3466.1766
- Seyf, H. R., and Rassoulinejad-Mousavi, S. M. (2011). An analytical study for fluid flow in a porous media imbedded inside a channel with moving or stationary walls subjected to injection/suction. *J. Fluids Eng.* 133, 091203. doi:10.1115/1.4004822
- Shah, S. L., Ayub, A., Dehraj, S., Wahab, H. A., Sagayam, K. M., Ali, M. R., et al. (2022). Magnetic dipole aspect of binary chemical reactive Cross nanofluid and heat transport over composite cylindrical panels. *Waves Random Complex Media* 12, 1–24. doi:10.1080/17455030.2021.2020373
- Shah, S. Z. H., Ayub, A., Sabir, Z., Adel, W., Shah, N. A., and Yook, S. J. (2021). Insight into the dynamics of time-dependent cross nanofluid on a melting surface subject to cubic autocatalysis. *Case Stud. Therm. Eng.* 27, 101227. doi:10.1016/j.csite.2021.101227
- Shah, S. Z. H., Fathurrochman, I., Ayub, A., Altamirano, G. C., Rizwan, A., Núñez, R. A. S., et al. (2022). Inclined magnetized and energy transportation aspect of infinite shear rate viscosity model of Carreau nanofluid with multiple features over wedge geometry. *Heat. Trans.* 51 (2), 1622–1648. doi:10.1002/htj.22367
- Shah, Z., Islam, S., Ayaz, H., and Khan, S. (2019). Radiative heat and mass transfer analysis of micropolar nanofluid flow of Casson fluid between two rotating parallel plates with effects of Hall current. *J. Heat Transf.* 141 (2), 022401. doi:10.1115/1.4040415
- Shah, Z., Khan, A., Khan, W., Alam, M. K., Islam, S., Kumam, P., et al. (2020). Micropolar gold blood nanofluid flow and radiative heat transfer between permeable channels. *Comput. methods programs Biomed.* 186, 105197. doi:10.1016/j.cmpb.2019.105197
- Sheikholeslami, M., and Ganji, D. D. (2013). Heat transfer of Cu-water nanofluid flow between parallel plates. *Powder Technol.* 235, 873–879. doi:10.1016/j.powtec.2012.11.030
- Singkidub, P., Sabir, Z., Al Nuwairan, M., Sadat, R., and Ali, M. R. (2022). Cubic autocatalysis-based activation energy and thermophoretic diffusion effects of steady micro-polar nano-fluid. *Microfluid. Nanofluidics* 26 (7), 50–12. doi:10.1007/s10404-022-02554-y
- Srinivas, S., Vijayalakshmi, A., Ramamohan, T. R., and Reddy, A. S. (2014). Hydromagnetic flow of a nanofluid in a porous channel with expanding or contracting walls. *J. Porous Media* 17 (11), 953–967. doi:10.1615/jpormedia.v17.i11.20
- Srinivas, S., Vijayalakshmi, A., and Subramanyam Reddy, A. (2017). Flow and heat transfer of gold-blood nanofluid in a porous channel with moving/stationary walls. *J. Mech.* 33 (3), 395–404. doi:10.1017/jmech.2016.102
- Tzirtzilakis, E. E. (2005). A mathematical model for blood flow in magnetic field. *Phys. fluids* 17 (7), 077103. doi:10.1063/1.1978807
- Zhang, C., Zheng, L., Zhang, X., and Chen, G. (2015). MHD flow and radiation heat transfer of nanofluids in porous media with variable surface heat flux and chemical reaction. *Appl. Math. Model.* 39 (1), 165–181. doi:10.1016/j.apm.2014.05.023
- Zhang, L., Arain, M. B., Bhatti, M. M., Zeeshan, A., and Hal-Sulami, H. (2020). Effects of magnetic Reynolds number on swimming of gyrotactic microorganisms between rotating circular plates filled with nanofluids. *Appl. Math. Mech.* 41 (4), 637–654. doi:10.1007/s10483-020-2599-7